Langmuir

Article

pubs.acs.org/Langmuir

Microrheology and Microstructure of Fmoc-Derivative Hydrogels

Anders Aufderhorst-Roberts,*[†] William J. Frith,[‡] Mark Kirkland,[‡] and Athene M. Donald[†]

[†]Cavendish Laboratory, Department of Physics, University of Cambridge, JJ Thomson Avenue, Cambridge, CB3 0HE U.K.

[‡]Unilever R&D, Colworth Science Park, Sharnbrook, Bedford, MK44 1LQ, U.K.

ABSTRACT: The viscoelasticity of hydrogel networks formed from the low-molecular-weight hydrogelator Fmoc-tyrosine (Fmoc-Y) is probed using particle-tracking microrheology. Gelation is initiated by adding glucono-δ-lactone (GdL), which gradually lowers the pH with time, allowing the dynamic properties of gelation to be examined. Consecutive plots of probe particle mean square displacement (MSD) versus lag time τ are shown to be superimposable, demonstrating the formation of a self-similar hydrogel network through a percolation transition. The analysis of this superposition yields a gel time $t_{gel} = 43.4 \pm 0.05$ min and a critical relaxation exponent $n_c = 0.782 \pm 0.007$, which is close to the predicted value of $^3/_4$ for semiflexible polymer networks. The generalized Stokes−Einstein relation is applied to the master curves to find the viscoelastic moduli of the critical gel over a wide frequency range, showing that the critical gel is structurally and rheologically fragile. The scaling of G'/G'' as $\omega^{0.795\pm0.099} \approx \omega^{3/4}$ at high frequencies provides further evidence for semiflexible behavior. Cryogenic scanning electron micrographs depict a loosely connected network close to the gel point with a fibrillar persistence length that is longer than the network mesh size, further indications of semiflexible behavior. The system reported here is one of a number of synthetic systems shown to exhibit semiflexible behavior and indicates the opportunity for further rheological study of other Fmoc derivatives.

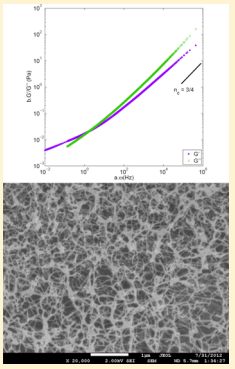

INTRODUCTION

The formation of hydrogels from low-molecular-weight components through physical cross-linking is an attractive strategy for the practical design of materials for applications such as wound treatment,[1] drug delivery,[2] and tissue engineering.[3] Networks formed from so-called low-molecular-weight hydrogelators (LMWH) exhibit a range of interesting features, including well-ordered structure, thermoreversibility, and a low critical gelation concentration.[4] LMWHs also have obvious advantages over more complex systems in so much as they are cheaper, faster, and easier to manufacture.

In recent years, increasing numbers of LMWHs have been reported as their discovery has begun to depend more upon rational design and less upon serendipity.[5] In particular, there is now a large body of work relating to peptide hydrogelators such as peptide amphiphiles,[6] beta hairpins,[7] coiled coils,[8] and peptides coupled to aromatic moieties such as fluorenylmethylcarboxyl (Fmoc),[9] pyrene,[10] and naphthalene[11] as well as Fmoc-amino acids[12] and mixtures of different amino acids.[13] Although the proposed applications[14] and chemical properties[9] of Fmoc-based systems have been well studied, there has been very little research on their rheological properties and the relation of these properties to microstructural characteristics and how both vary dynamically during gel formation. Where such properties have been investigated, the method used has generally been some form of oscillatory bulk rheology.[15,16] However, this approach has several limitations: the time taken to perform a frequency sweep prevents the study of rapidly evolving samples, and in any case, the accessible frequency range over which viscoelastic moduli can be measured is limited.

Microrheology is a collection of techniques that determine the viscoelastic moduli of soft materials from the Brownian motion of embedded probe particles. This can be achieved through optical trapping,[17] magnetic trapping,[18] light scattering,[19] and video particle tracking.[20] A particular advantage of particle-tracking microrheology (PTM) is the comparably fast rate of measurements that can be achieved and the wide dynamic frequency range, which is limited only by the data acquisition rate of the camera and the speed of data storage.[21] The raw data collected by PTM is the ensemble-average mean-squared displacement (MSD) of embedded particles, which can be examined directly or converted into frequency-dependent viscoelastic moduli via the well-established generalized Stokes−Einstein relation (GSER)

$$G(s) = \frac{2k_BT}{3\pi as\langle \Delta r(s)^2 \rangle} \quad (1)$$

where s is the Laplace frequency and $G(s)$ and $\langle r(s)^2 \rangle$ are the Laplace transforms of the complex modulus and MSD, respectively. A recent innovation[22] has been the application of time-cure superposition to microrheological data. As gelation occurs, the self-similar nature of the evolving network means that, whereas the characteristic length scale of the network changes, its shape and structure do not. Hence, the MSD scales vertically and horizontally as the characteristic time scales and creep compliance diverge at the gel point,[23] allowing a so-called MSD master curve to be constructed. This approach is useful for a number of reasons. First, it allows the precise gel point

Received: February 12, 2014
Revised: March 25, 2014
Published: March 31, 2014

   dx.doi.org/10.1021/la5005819 | *Langmuir* 2014, 30, 4483−4492

(the time it takes for an infinite network to appear[24]) to be calculated through analyzing the divergence of the shift factor used to superimpose the MSD curves.[25] Second, the GSER can be applied directly to the MSD master curve, yielding the viscoelastic moduli over a greatly increased frequency range.[26] Finally, the power law exponent of the MSD at the calculated gel time, also known as the critical exponent n_c, can be found. The critical exponent has a theoretical range of $0 < n_c < 1$,[27] and values of n_c have been observed across almost all of this range. Practically speaking, the value of n_c can be said to provide an indication of the microstructural properties of the gel network. In chemically cross-linking systems, the value of n_c has been shown to decrease with increasing concentration of cross-linker,[27] whereas in physical gels a large value of n_c can be correlated with a critical gel that is weak and fragile.[28] Values of n_c can also be compared to predicted values from different polymer theories, thereby characterizing their behavior. Flexible polymeric fractal gels formed from LMWH are expected to follow Rouse's theory of screened hydrodynamic interactions ($n_c \approx {}^2/_3$)),[29] although recent studies of a variety of physically cross-linking systems have shown minor deviations from this value,[30,22] and it has been postulated that the discrepancy can be attributed to a bond probability that changes with time.[44]

In this study, the gelation behavior of Fmoc-tyrosine (Fmoc-Y), an LMWH, is studied using particle-tracking microrheology. To trigger gelation, glucono-δ-lactone (GdL) is added, which gradually lowers the pH, thereby bringing about gelation at a controllable rate. Time-cure superposition is used to construct an MSD master curve, allowing the precise gel point t_{gel} and the critical exponent n_c to be determined. The GSER is applied to the MSD master curves to give values of G'/G'' over a wide frequency range. To complement microrheology, the hydrogel network morphology is examined directly through cryogenic scanning electron microscopy (cryo-SEM).

EXPERIMENTAL SECTION

Materials. All materials were purchased from Sigma-Aldrich, and Millipore water was used throughout.

Sample Preparation. Fmoc-Y-OH ((42 mg, 0.104 mmol) is weighed into a glass vial. Sodium hydroxide (10 mL of a 0.0004% w/v solution, 0.1 mmol) is then added. To aid dissolution, the resulting solution is gently warmed to 40 °C and agitated. Agitation and dissolution are repeated until the solution reaches pH 8. Because of the inherently stochastic nature of the gelation process[31] and the fact that the Fmoc moiety is known to be unstable under alkaline conditions,[32] care is taken to ensure that samples are prepared at precisely this pH. Excess Fmoc-Y-OH is removed using a syringe filter with a 220 nm porous membrane, leaving a clear solution. To initiate gelation, a 3 mL aliquot of this solution is then added to GdL powder (5.34 mg, equivalent to 10 mM GdL) and mixed by shaking vigorously for 20 s. The resulting hydrolysis of GdL leads to the formation of gluconic acid via a series of intermediate steps.[33] Hence, the pH decreases gradually and gelation occurs over time. The molecular structures of Fmoc-Y and GdL (and its transition to gluconic acid) are shown in Figure 1.

pH Measurements. A Thermoscientific Orion 3star benchtop pH meter equipped with a Fischer Scientific pH probe is used to measure the pH. The pH meter is connected via a serial cable to a PC, allowing pH measurements to be automated by taking readings every 10 s. The pH meter is calibrated before each experiment to check the response of the electrode with two buffer solutions purchased from Fisher Scientific (borate at pH 10 and phosphate at pH 7).

Particle-Tracking Microrheology. Following the preparation of Fmoc-Y in solution but before GdL is added, latex polystyrene particles of diameter 0.46 μm are immediately added to the sample. All probe particles were purchased from Sigma-Aldrich. The particles have

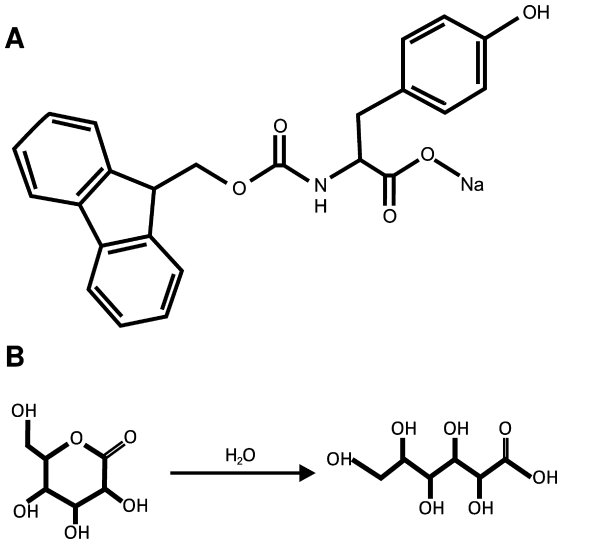

Figure 1. Molecular structures of the gelling material and gelation agent. (A) The salt form of Fmoc-Y is used because it is significantly more soluble in water than its acid form. (B) Glucono-δ-lactone hydrolyses through a series of complex chemical equilibrium to form gluconic acid, thereby lowering the pH gradually.

unmodified surface chemistry, and their volume fraction in the sample is 0.01%. Following the addition of probe particles, a 40 μL aliquot of the sample is added to an aluminum sample cell of depth 1.2 mm. The sample temperature is maintained at 25 °C throughout by the use of a Peltier chip heating stage comprising a thermoelectric module with a hole in the center sandwiched between a copper sample holder and a brass heat sink. Temperature is controlled by modifying the voltage across the thermoelectric module, and feedback is facilitated by a thermocouple embedded in the sample holder.

The Brownian motion of probe particles is visualized using a Zeiss Axioplan LSM 500 confocal microscope operating in bright-field mode. Videos are captured using an AVT Pike CCD camera. During tracking, different objectives (32× and 50×) are used, and the objective size is varied according to the diffusivity of the probe particles. The frame rate is also varied within the range of 30−120 s^{-1} to account for different particle diffusivities. The exposure time of the CCD camera is kept to a minimum to ensure that particle movement within the duration of each video frame is minimized. A static error, representing the tracking resolution of the technique, that manifests itself as a constant additive term in the particle mean-squared displacement (MSD) is also present.[34] This error can be measured most reliably by fitting a straight line to plots of the MSD versus lag time τ.[35] The static error is simply the value at which this fitted line intercepts the y axis, although its value is likely to vary with incubation time t_w as a result of changes in the sample turbidity. Hence, the estimation of the static error by this method is approximate. However, in this study the measured magnitude of this error is found to be several orders of magnitude smaller than the measured MSD within the time scale that data is collected. Hence, it can be assumed that the static error has a negligible effect on the measurements of the MSD.

Videos are captured in a lossless avi format using AVT Amcap (part of the AVT Direct Stream Package) and converted into a series of bitmap images using VirtualDub, a free video-processing software package. Image analysis is carried out using in-house custom-written Matlab scripts.[36] Particle positions in individual frames are identified using a standard computational process for edge detection in images known as a Laplacian-of-Gaussian operation.[37] This involves smoothing the image by using a Gaussian filter and then applying a Laplacian filter to detect particle edges. Particle centroid positions are calculated by applying a double-quadratic fit, and background noise in the images is then reduced by systematically removing pixels whose intensity is below a manually defined intensity threshold.

dx.doi.org/10.1021/la5005819 | Langmuir 2014, 30, 4483−4492

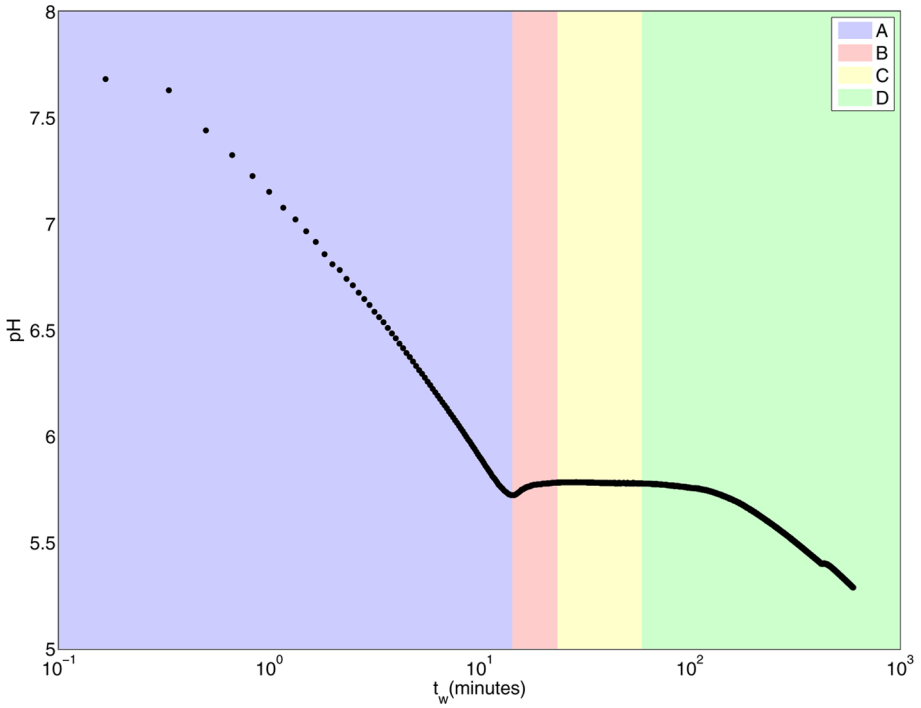

Figure 2. pH vs t_w for a hydrogel sample prepared using 10 mM Fmoc-Y and 10 mM GdL. Although there is a significant amount of variability between measurements of pH with respect to time, the pattern of evolution of pH is broadly consistent and follows four steps, marked by colored regions. In step A, the pH drops sharply before rising briefly in step B and buffering in step C. At longer time scales, labeled as step D, the pH continues to drop, albeit more gradually.

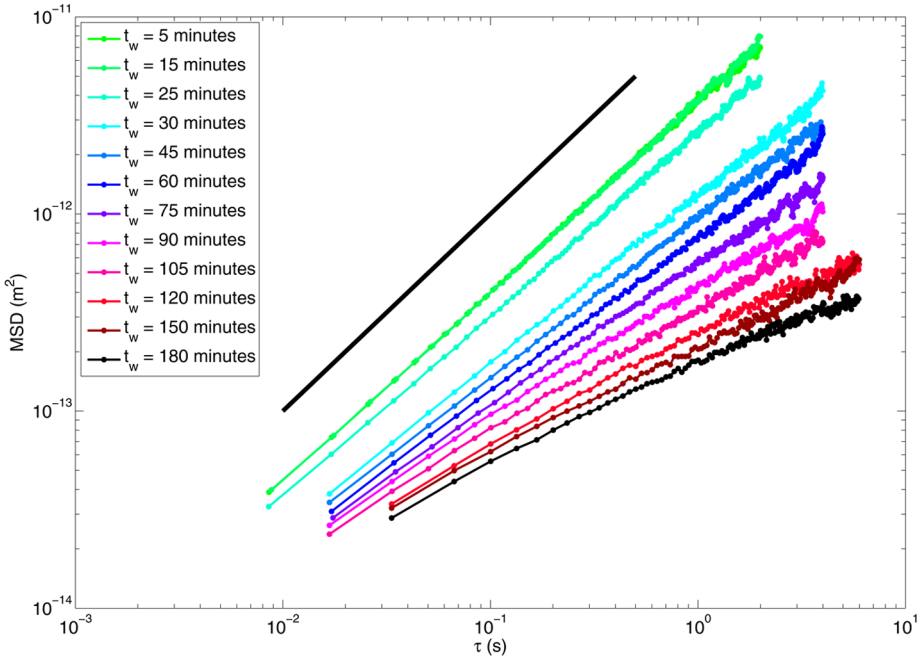

Figure 3. Selected plots of MSD with respect to lag time τ at selected incubation time t_w for a hydrogel sample prepared from 10 mM Fmoc-Y and 10 mM GdL. At early t_w, MSD appears to remain invariant with a power law exponent of approximately 1. Both the magnitude of the MSD and the power law exponent later begin to drop as the viscosity of the sample increases. At some later t_w, the MSD exhibits subdiffusive behavior with τ across all lag times, indicating that a sample-spanning hydrogel network has formed. The solid black line indicates a power law exponent of 1.

Theoretically, the ensemble-averaged mean of the particle displacements caused by Brownian motion can be expected to be negligible. A significant ensemble-averaged particle displacement indicates bulk drift caused by external vibrations, temperature convection, or bulk relaxation in the sample. Therefore, particle displacements are monitored over 100-frame increments, and any particle movement that is common to the ensemble of particles is manually subtracted to correct for bulk drift. From the trajectories, the 2D mean-squared displacement is calculated and analyzed further. The viscous and elastic moduli can be calculated from the 2D mean-squared displacement using the GSER. Because the data range of MSD is

dx.doi.org/10.1021/la5005819 | *Langmuir* 2014, 30, 4483−4492

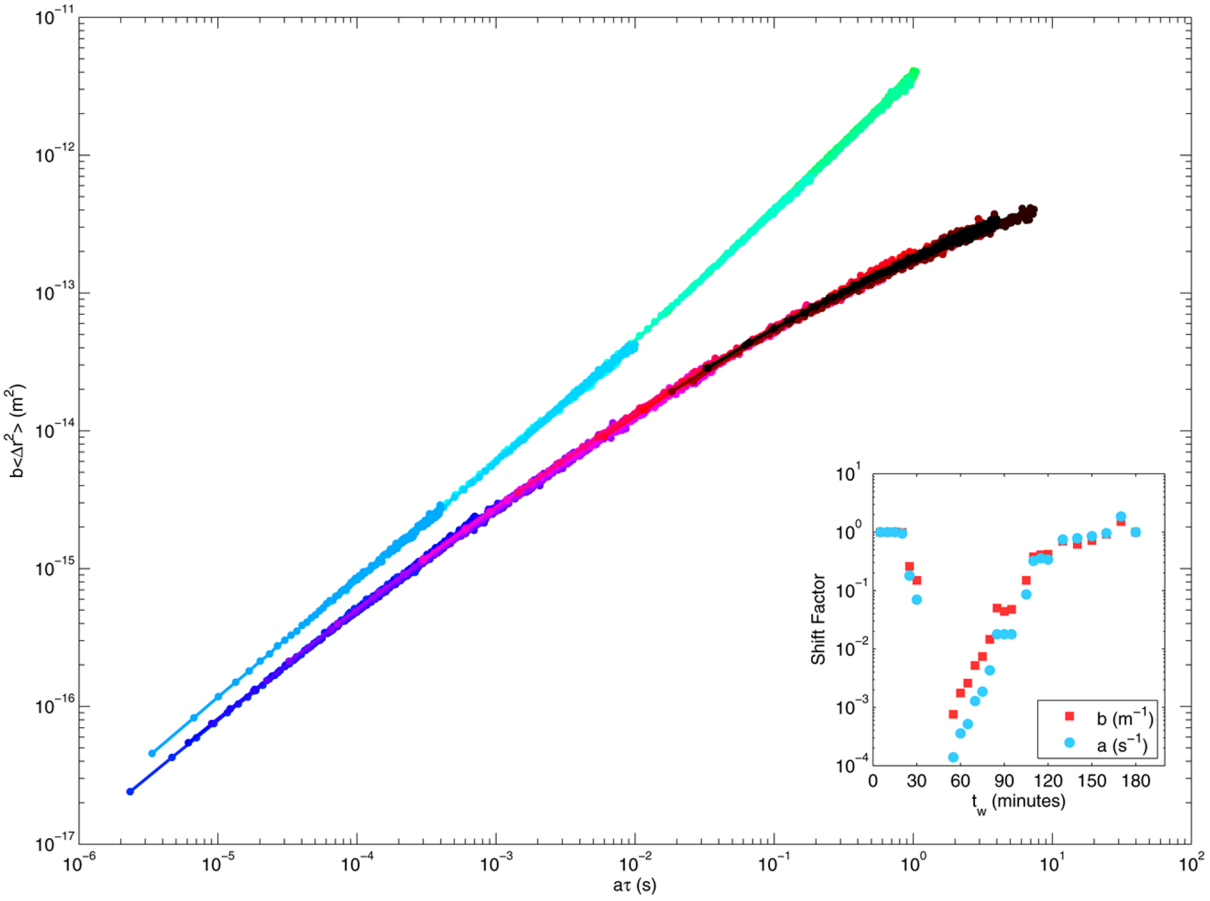

Figure 4. Master curves derived by applying arbitrary horizontal (a) and vertical (b) shift factors to MSD curves at a range of t_w for a hydrogel sample prepared from 10 mM Fmoc-Y and 10 mM GdL. Master curves are formed from postgel (bottom) and pregel (top) data. Different colors indicate different values of t_w. The inset shows horizontal and vertical shifts plotted with respect to t_w. Because a and b are inversely proportional to the longest relaxation time of the aggregate clusters and the hydrogel's creep compliance, respectively, both of which tend to infinity at t_{gel},[23] they both diverge at t_{gel}.

finite, the GSER is instead applied to analytically derived second-order time derivatives of the MSDs as reported by Dasgupta et al.[38]

Cryogenic Scanning Electron Microscopy. Following the preparation of Fmoc-Y, a 6 μL aliquot of sample is pipetted into a brass rivet with a 1 mm internal diameter. The rivet is stored in a high-humidity environment to prevent evaporation until a desired incubation time is reached. The sample is then mounted onto a cooled sample holder and plunged into nitrogen slush at −196 °C. Following freezing, the sample is transferred to a Gatan Alto 2500 preparation chamber at −120 °C and fractured using a scalpel. The fracture angle is chosen carefully to ensure that the resulting exposed region of the gel is closest to the edge of the sample, the position at which freezing occurs at the fastest rate and therefore at which the smallest ice crystals form. Once fractured, the sample is coated with a 2 nm layer of platinum−palladium to reduce charging and improve signal generation.

RESULTS AND DISCUSSION

pH Measurements. The evolution of pH with respect to incubation time t_w at a given concentration is highly variable between measurements because of the highly stochastic nature of the hydrolysis of GdL. However, there is uniformity in the pattern of evolution of pH, which can be described by the following four steps: (A) as soon as the GdL is added, the pH immediately drops sharply, (B) at some intermediate t_w, the pH briefly increases by a small amount, (C) the pH is invariant with time as buffering occurs, (D) at later t_w, the pH gradually begins to decease again.

Figure 2 shows a sample curve of pH versus t_w with each of these four steps clearly marked. This unusual pattern of pH evolution, particularly the drop and subsequent rise in steps A and B, has been reported in a number of similar systems[31] and has been postulated to be due to either a supersaturation of molecules in solution, which begin to self-assemble after step B, or the fact that the pK_a of the self-assembled form of Fmoc-Y is higher than the pK_a of the sol form of Fmoc-Y, causing an increase in the pH when aggregation begins.[15] Both of these theories would suggest that the transition between steps A and B correlates to the onset of aggregation. This transition is found, through repeat experiments, to be 16.6 ± 11.2 min.

Particle Tracking. Figure 3 shows the probe particle 2D mean-squared displacement (MSD) with respect to lag time τ at selected values of t_w.

MSD is found to follow a constant power law with a τ relationship at early t_w, with exponent α = 1 indicating a classical Newtonian fluid. As t_w increases, the magnitude of the MSD initially remains unchanged, suggesting that aggregation has not begun. As t_w increases further, MSD begins to drop at all measured τ as does the power law exponent (from α = 1 at t_w = 15 min to 0.798 at t_w = 25 min, over all measured τ). The drop in MSD for t_w = 15−25 min is consistent with predictions of the onset of aggregation from Figure 2.

dx.doi.org/10.1021/la5005819 | Langmuir 2014, 30, 4483−4492

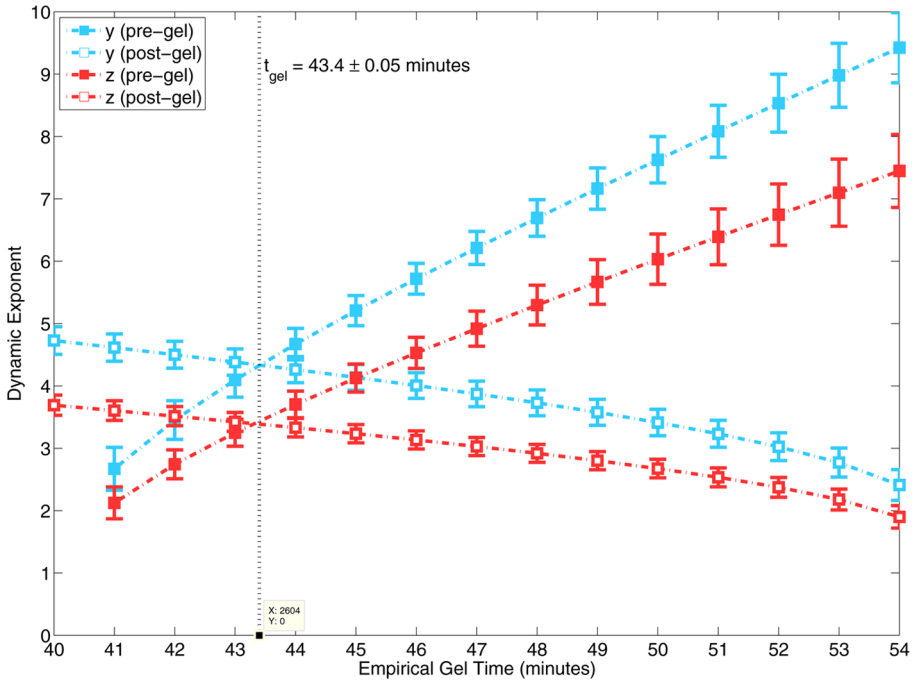

Figure 5. Analytical determination of the gel point. Empirically calculated dynamic exponents y and z for pregel (filled circles) and postgel (open circles) are shown for different manually chosen t_{gel} values. The point at which postgel and pregel data align is the gel point, t_{gel} = 43.4 min, which corresponds to dynamic exponents of y = 4.33 ± 0.48 and z = 3.39 ± 0.36.

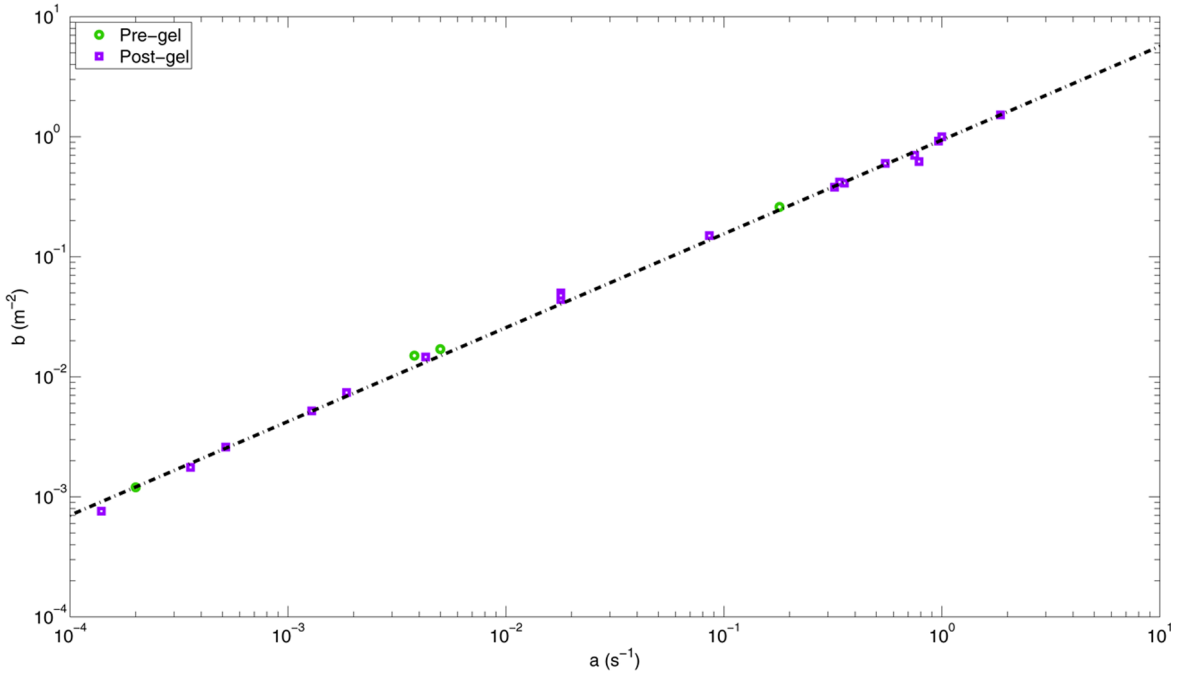

Figure 6. Analytical determination of n_c. The value of n_c is calculated as the logarithmic gradient of plots of the shift factors a and b, giving a value of n_c = 0.782 ± 0.007, which is independent of the calculated value of t_{gel} shown in Figure 5.

The decrease in α indicates subdiffusive dynamics in the probe particle trajectories resulting from the relaxation of growing aggregate clusters in solution, a phenomenon predicted by Rouse theory.[39] However, because α is not dependent on τ, the sample can be said to be a continuum over the length scales probed by the particles. At later t_w, the MSD begins to curve downward with respect to τ, indicating the formation of a sample-spanning network. In agreement with previous studies under the same conditions,[40] this is found to occur at approximately $t_w \approx 50-60$ min.

Through the principles of time-cure superposition,[23] MSD curves are superimposed on a master curve. This is achieved by multiplying individual curves by a time-shift factor a and an MSD shift factor b. Shift factors are manually chosen to ensure the best possible superposition of curves so that their logarithmic gradients superimpose. There are two master curves, pregel and postgel. Figure 4 shows the superimposed

dx.doi.org/10.1021/la5005819 | Langmuir 2014, 30, 4483−4492

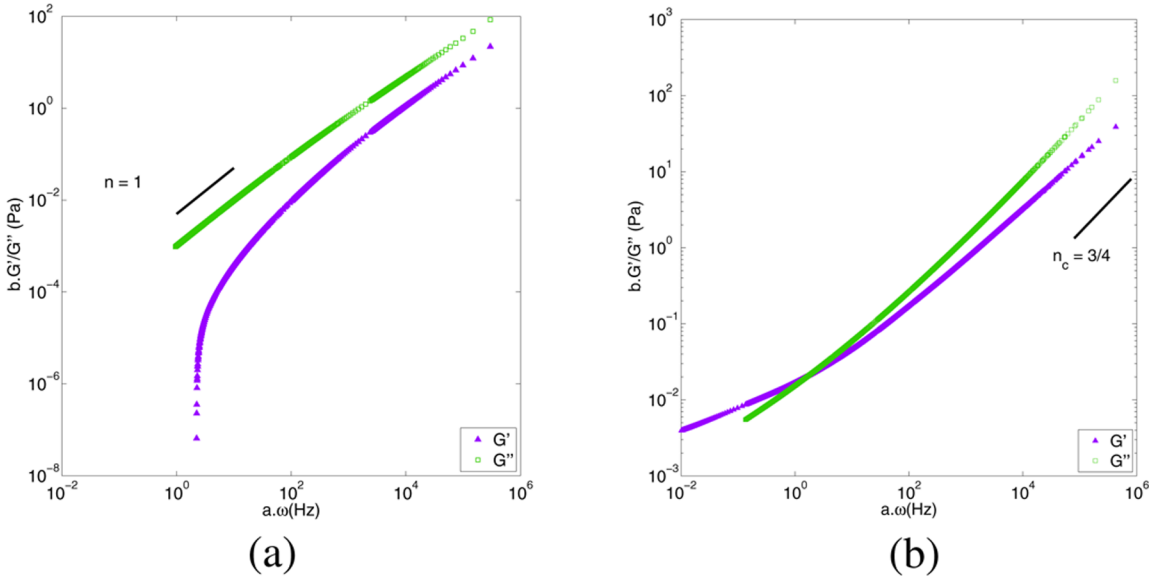

Figure 7. Elastic (G') and viscous (G'') moduli with respect to frequency for pregel (a) and postgel (b) systems calculated from the superimposed MSD master curves in Figure 4. Pregel trends in both moduli indicate that the system is broadly viscous over all frequencies. Postgel, the system is dominated by a viscous response over a wide range of frequencies; however, the elastic response is dominant at particularly low frequencies, confirming that the hydrogel is weak and incipient over the range of incubation times studied. Both pregel and postgel systems exhibit an approximate scaling of $G'/G'' \propto \omega^{3/4}$ at high frequencies, a behavior characteristic of semiflexible systems.

master curves that result from this process. Superposition is particularly effective for postgel MSD curves. Superposition is less effective at pregel incubation times because there are a smaller number of superimposed curves and the fact that their individual gradients are similar over all τ makes the process of superimposition somewhat uncertain. Shift factors a and b are inversely proportional to the longest relaxation time of the hydrogel network and the creep compliance, respectively.[22] Because both of these properties are known to diverge to infinity at t_{gel}, a and b can be predicted to diverge to zero.[23] This divergence is shown in the inset of Figure 4, where a and b are plotted with respect to t_w. The divergence of a and b is predicted to be symmetrical around the sol−gel transition such that[30]

$$a(\varepsilon) \propto \varepsilon^{y}, \quad b(\varepsilon) \propto \varepsilon^{z} \tag{2}$$

where ε is a measure of the distance in t_w from the percolation transition

$$\varepsilon = \frac{|p - p_c|}{p_c} = \frac{|t_w - t_{gel}|}{t_{gel}} \tag{3}$$

where p is the bond probability between gelling components and p_c is the critical bond probability required to bring about gelation. Values of y and z can be calculated by choosing different values of t_{gel} in order to give different values of ε and thus different values of y and z. The symmetry of the sol−gel transition means that postgel and pregel values of y and z are equal, thus allowing the precise value of t_{gel} to be identified as 43.4 ± 0.05 min and also giving values of y = 4.33 ± 0.48 and z = 3.39 ± 0.36 as shown in Figure 5.

The power law exponent of the MSD at t_{gel}, known as the critical exponent n_c, can be determined using one of two methods. The first method is to use the relation $n_c = {}^{z}/_{y}$,[23] which gives n_c = 0.783 ± 0.170. However, the associated error in n_c when this method is used is relatively high as a result ofthe propagated errors from the estimated values of y and z. A more precise method is to find n_c independently of y and z by substituting $n_c = {}^{z}/_{y}$ into eq 2 to give

$$n_c \propto \frac{\log(a(\varepsilon))}{\log(b(\varepsilon))} \tag{4}$$

and applying a linear fit to a plot of $\log(a)$ versus $\log(b)$, giving n_c = 0.782 ± 0.007 as shown in Figure 6.

As expected, the value of n_c calculated through this method is in close agreement with the value calculated using $n_c = {}^{z}/_{y}$. When compared to previously reported values of n_c in the literature, we find that the value of n_c measured here is particularly high, indicative of a gel network at the critical point of gelation that is weak and fragile and whose aggregate components undergo rapid relaxation under stress.[28]

The value of n_c can be compared to predictions from established polymer theories. Neither the value of n_c = 0.66 predicted by Rouse[41] (assuming screened hydrodynamic interactions) nor the value of n_c = 1 predicted by Zimm theory[42] (unscreened hydrodynamic interactions) is in agreement with the experimentally determined value of ∼0.78. A better approximation is given by the semiflexible polymer model, which predicts $n_c \approx {}^{3}/_{4}$ at high frequencies.[43] The small deviation from this predicted value can be attributed to the fact that the divergence of shift factors a and b (inset, Figure 4) does not appear to be perfectly exponential with lag time. This imperfect divergence indicates that the assumption that the bond probability, p, is directly proportional to t_w may be questionable,[44] an observation consistent with findings in other physically gelling systems.[22,30]

Viscoelastic Moduli. The GSER (eq 1) is applied to the MSD master curves shown in Figure 4 to create master curves in G' and G'' for both pregel and postgel states, which are reliable over several decades of frequency.[26] These are shown in Figure 7. To avoid truncation errors at frequency extremes[45] and thus maximize the dynamic range, the moduli are calculated by applying a Laplace transform to a functional

dx.doi.org/10.1021/la5005819 | Langmuir 2014, 30, 4483−4492

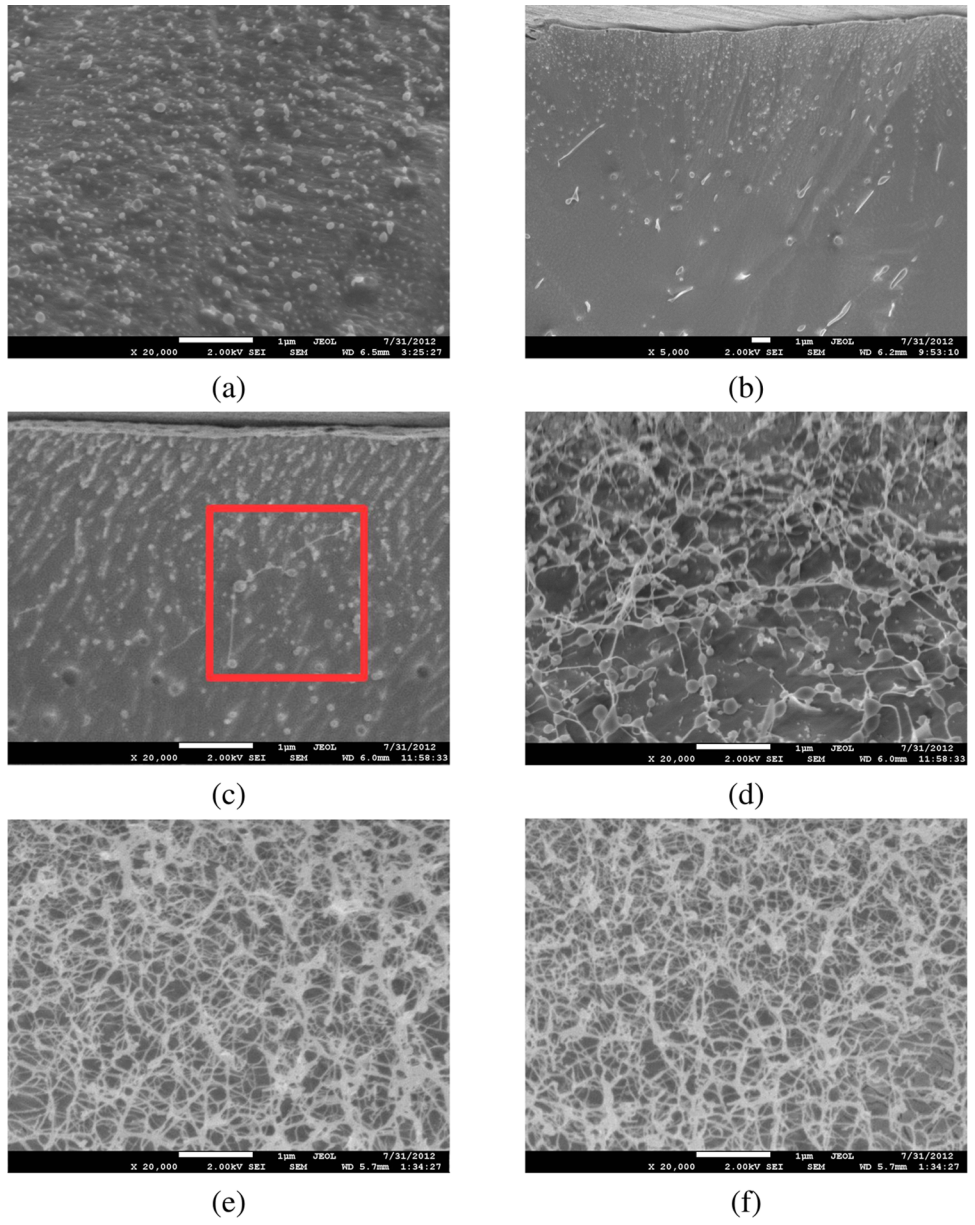

Figure 8. Cryo-SEM micrographs at selected t_w. Before the addition of GdL (a), spherelike aggregated structures can be clearly seen. Because the sample is prepared without the addition of GdL, these structures can be assumed to be artifacts arising from cryogenic freezing, and their presence in subsequent cryo-SEM micrographs can be discounted. At t_w = 0 min, no aggregation takes place (b), whereas by t_w = 15 min (c), isolated fibrillar aggregates, with length on the order of hundreds of nanometers can be seen (as highlighted by the red boxes). Fibrillar aggregates increase in density and begin to entangle at t_w = 30 min (d) such that at t_w = 1 h (e) and t_w = 2 h (f) a loosely connected gel network has formed with a mesh size of the length scale on the order of tens of nanometers, clearly indicating that gelation has taken place. This loose connectivity is consistent with the high measured value of n_c, which indicates that the gel network is initially weak, whereas the high persistence length of the fibrillar aggregates in comparison to the length scale of the hydrogel mesh is consistent with semiflexible polymer theory.[46] At t_w = 2 h, the fibers coarsen. Scale bars are shown in each individual subfigure.

form of the MSD that includes a second-order logarithmic MSD time derivative term.[38]

Figure 7 shows that before the gel point the response of the system is broadly viscous over all frequencies. At the lower end of the frequency range ($a\omega$ < 10 Hz), G' drops abruptly. This phenomenon is artificial and caused by truncation errors in the application of the GSER resulting from the finite frequency range of the data. The logarithmic gradient of pregel G'' (Figure 7a) tends to 1 at low frequencies, indicating purely viscous behavior at long length scales. For the postgel master curves of G' and G'' (Figure 7b), the values of G' and G'' cross over at low frequencies, with G' approaching a plateau with respect to frequency. The low frequency at which this crossover occurs indicates that the response of the hydrogel network retains a significant viscous component after the gel point, a finding that correlates well with the previously measured high value of n_c, as both findings indicate a weak, fragile hydrogel network.

At high frequencies in postgel systems, the logarithmic gradients of G'/G'' are found to tend toward 0.795 ± 0.099, a value close to the value of $^3/_4$ predicted for semiflexible systems. The error margin here is larger than the scaling calculated from plots of MSD versus τ as a result of the

dx.doi.org/10.1021/la5005819 | Langmuir 2014, 30, 4483−4492

approximate nature of the GSER. The observation that G' increases with frequency is also indicative of an entangled gel mesh, without permanent cross-links.[43]

Cryo-SEM. To investigate any artifacts that may be inherent in the technique, cryo-SEM is applied to a hydrogel sample prepared using 10 mM Fmoc-Y but without the addition of GdL. The micrograph in Figure 8a clearly shows the presence of spheroid aggregate structures. The fact that they are observed here for a sample where aggregation can be assumed not to have occurred should be taken as an indication that they are artifacts associated with the cryogenic freezing process. It should be emphasized that this does not mean that such aggregates do not form in the case of Fmoc-Y but rather that cryo-SEM is not an effective way of detecting them. Cryo-SEM micrographs of gelling samples at a range of incubation times are shown in Figure 8b–f.

At t_w = 0 min (Figure 8b), there is no evidence of any aggregation, although low densities of aggregate clusters of similar size and shape to those shown in Figure 8a are apparent. These can therefore be discounted as artifacts. At t_w = 15 min (Figure 8c), these artifacts are still present, but the presence of small but clearly defined fibrils can also be seen, with an apparent length on the order of hundreds of nanometers (highlighted in the region bounded by a red box). The small size of the fibrils and their relatively low concentration are consistent with the interpretation of MSD curves in Figure 3, in which the aggregates were surmised to be insufficiently large to be probed by embedded particles. The early signs of aggregation on this time scale are also consistent with both the invariance in the MSD at t_w < 15–25 min (Figure 3) and with the prediction of the onset of aggregation at 16.6 ± 11.2 min from pH measurements (Figure 2).

At t_w = 30 min (Figure 8d), the fibrils increase in density and begin to entangle, forming a coarse, loosely percolated hydrogel network at t_w = 60 min (Figure 8e) whose fibers become thicker at later incubation times (t_w = 2 h, Figure 8f). Percolation of the gel network is observed at an incubation time relatively close to the previously measured t_{gel}. This observation is consistent with the relatively high previously measured value of n_c that predicts that the hydrogel network should be relatively weak and fragile at the gel point. From a visual examination, network fibers have a thickness of approximately 10–30 nm with a mesh size on the order of tens of nanometers. It should be stressed that these figures are highly approximate as the platinum–palladium coating of the sample artificially increases the apparent fiber thickness, thereby also decreasing the mesh size. The fact that the mesh size of the network is clearly smaller than the persistence length of the fibers is also characteristic of semiflexible polymer filaments.[46]

CONCLUSIONS

Self-similar behavior is observed for hydrogels formed from the LMWH Fmoc-Y. Time-cure superposition is successfully applied to the MSD curves using the method of Larsen and Furst.[22] The resulting calculated critical exponent n_c = 0.782 ± 0.007 indicates that the gel network can be described as semiflexible, although there are slight discrepancies between experiment and theory, a likely result of a percolation bond probability that varies with t_w.[44] Further evidence for semiflexible behavior can be seen in plots of G'/G'', both of which scale as approximately $\omega^{3/4}$ at high frequencies and tend to plateau at low frequencies. Further supporting data can be seen as well as the morphology of the network as measured through cryo-SEM, which shows the persistence length of fibrillar aggregates to be greater than the entanglement length of the hydrogel network. Theoretical models for semiflexible networks have been devised,[47] which relate the pore size of the gel mesh, the viscoelastic moduli, and microstructural properties such as the entanglement length and the persistence length of individual fibers. It should be possible, through more detailed investigation, to derive these microstructural properties using the techniques described here, and we intend this to be the subject of future work.

The weak nature of the hydrogel network makes it ideal for study through microrheology as the presence of static errors in the MSD prevent the use of microrheology for particularly stiff gels.[34] However, the measured viscoelastic moduli stand in contrast to bulk rheological studies of Fmoc-Y at later incubation times.[48] This presents an opportunity for future work to study the rheological properties of Fmoc-Y over a range of different length scales and time scales.

Finally, although a wide range of synthetic peptide systems have been studied in the literature, only a few have been rheologically characterized as either flexible[22] or semiflexible.[49−51] The authors postulate that analogous systems such as Fmoc-dipeptides may also exhibit semiflexible behavior, but that this has yet to be reported because of the lack of frequency dependence of G' measured by the limited frequency range of oscillatory rheometry.[31] Microrheology would therefore also be a useful tool for further elucidating the properties of Fmoc-dipeptides. Such work could also exploit alternative gelation triggers such as enzyme thermolysin, which has been shown to induce gelation in a highly reproducible manner under thermodynamic control.[52]

AUTHOR INFORMATION

Corresponding Author

*E-mail: a.aufderhorst-roberts@leeds.ac.uk.

Present Address

Anders Aufderhorst-Roberts: School of Physics & Astronomy, E. C. Stoner Building, University of Leeds, Woodhouse Lane, Leeds LS2 9JT, United Kingdom.

Notes

The authors declare no competing financial interest.

ACKNOWLEDGMENTS

This work formed part of the doctoral thesis of A.A-R. We gratefully acknowledge funding from the EPSRC and Unilever R&D through an EPSRC CASE studentship.[53]

REFERENCES

(1) Matson, J. B.; Zha, R. H.; Stupp, S. I. Peptide self-assembly for crafting functional biological materials. *Curr. Opin. Solid State Mater. Sci.* **2011**, *15*, 225–235.

(2) Discher, D. E.; Eisenberg, A. Polymer vesicles. *Science* **2002**, *297*, 967–973.

(3) Gelain, F.; Horii, A.; Zhang, S. Designer self-assembling peptide scaffolds for 3-D tissue cell cultures and regenerative medicine. *Macromol. Biosci.* **2007**, *7*, 544–551.

(4) Estroff, L.; Hamilton, A. Water gelation by small organic molecules. *ChemInform* **2004**, *35*, 1201–1217.

(5) de Loos, M.; Feringa, B. L.; van Esch, J. H. Design and application of self-assembled low molecular weight hydrogels. *Eur. J. Org. Chem.* **2005**, *2005*, 3615–3631.

(6) Hartgerink, J. D.; Beniash, E.; Stupp, S. I. Peptide-amphiphile nanofibers: A versatile scaffold for the preparation of self-assembling materials. *Proc. Natl. Acad. Sci. U.S.A.* **2002**, *99*, 5133−5138.
(7) Lamm, M. S.; Rajagopal, K.; Schneider, J. P.; Pochan, D. J. Laminated morphology of nontwisting beta-sheet fibrils constructed via peptide self-assembly. *J. Am. Chem. Soc.* **2005**, *127*, 16692−16700.
(8) Banwell, E. F.; Abelardo, E. S.; Adams, D. J.; Birchall, M. A.; Corrigan, A.; Donald, A. M.; Kirkland, M.; Serpell, L. C.; Butler, M. F.; Woolfson, D. N. Rational design and application of responsive [alpha]-helical peptide hydrogels. *Nat. Mater.* **2009**, *9*, 596−600.
(9) Smith, A. . M.; Williams, R. . J.; Tang, C.; Coppo, P.; Collins, R. . F.; Turner, M. . L.; Saiani, A.; Ulijn, R. V. Fmoc-Diphenylalanine self assembles to a hydrogel via a novel architecture based on $\pi-\pi$ interlocked β-sheets. *Adv. Mater.* **2008**, *20*, 37−41.
(10) Zhang, Y.; Yang, Z.; Yuan, F.; Gu, H.; Gao, P.; Xu, B. Molecular recognition remolds the self-assembly of hydrogelators and increases the elasticity of the hydrogel by 106-fold. *J. Am. Chem. Soc.* **2004**, *126*, 15028−15029.
(11) Yang, Z.; Liang, G.; Ma, M.; Gao, Y.; Xu, B. Conjugates of naphthalene and dipeptides produce molecular hydrogelators with high efficiency of hydrogelation and superhelical nanofibers. *J. Mater. Chem.* **2007**, *17*, 850−854.
(12) Yang, Z.; Gu, H.; Fu, P. D.; Gao, J. L.; Xu, B. Enzymatic formation of supramolecular hydrogels. *Adv. Mater.* **2004**, *16*, 1440−1444.
(13) Mann, S.; Schepp, Z.; Gonzalez-McQuire, R. Hybrid biocomposites based on calcium phosphate mineralization of self-assembled supramolecular hydrogels. *Adv. Mater.* **2006**, *18*, 1869−1872.
(14) Liebmann, T.; Rydholm, S.; Akpe, V.; Brismar, H. Self-assembling Fmoc dipeptide hydrogel for in situ 3D cell culturing. *BMC Biotechnol.* **2007**, *7*, 88.
(15) Tang, C.; Smith, A. M.; Collins, R. F.; Ulijn, R. V.; Saiani, A. Fmoc-Diphenylalanine self-assembly mechanism induces apparent pK_a shifts. *Langmuir* **2009**, *25*, 9447−9453.
(16) Mahler, A.; Reches, M.; Rechter, M.; Cohen, E.; Gazit Rigid, S. Self-assembled hydrogel composed of a modified aromatic dipeptide. *Adv. Mater.* **2006**, *18*, 1365−1370.
(17) Yao, A.; Tassieri, M.; Padgett, M.; Cooper, J. Microrheology with optical tweezers. *Lab Chip* **2009**, *9*, 2568−2575.
(18) Amblard, F.; Yurke, B.; Pargellis, A.; Leibler, S. A magnetic manipulator for studying local rheology and micromechanical properties of biological systems. *Rev. Sci. Instrum.* **1996**, *67*, 818−827.
(19) Mason, T. G.; Weitz, D. A. Optical measurements of frequency-dependent linear viscoelastic moduli of complex fluids. *Phys. Rev. Lett.* **1995**, *74*, 1250−1253.
(20) Mason, T. G.; Ganesan, K.; van Zanten, J. H.; Wirtz, D.; Kuo, S. C. Particle tracking microrheology of complex fluids. *Phys. Rev. Lett.* **1997**, *79*, 3282−3285.
(21) Waigh, T. A. Microrheology of complex fluids. *Rep. Prog. Phys.* **2005**, *68*, 685−742.
(22) Larsen, T. H.; Furst, E. M. Microrheology of the liquid-solid transition during gelation. *Phys. Rev. Lett.* **2008**, *100*, 146001.
(23) Adolf, D.; Martin, J. E. Time-cure superposition during crosslinking. *Macromolecules* **1990**, *23*, 3700−3704.
(24) Winter, H. H.; Mours, M. *Neutron Spin Echo Spectroscopy Viscoelasticity Rheology*; Advances in Polymer Science; Springer: Berlin, 1997; Vol. *134*, pp 165−234.
(25) Larsen, T.; Schultz, K.; Furst, E. M. Hydrogel microrheology near the liquid-solid transition. *Korea-Aust. Rheol. J.* **2008**, *20*, 165−173.
(26) Corrigan, A. M.; Donald, A. M. Passive microrheology of solvent-induced fibrillar protein network. *Langmuir* **2009**, *25*, 8599−8605.
(27) Chambon, F. Linear viscoelasticity at the gel point of a crosslinking PDMS with imbalanced stoichiometry. *J. Rheol.* **1987**, *31*, 683.
(28) Winter, H. H.; Izuka, A.; Rosa, M. E. D. Experimental observation of the molecular weight dependence of the critical exponents for the rheology near the gel point. *Polym. Gels Networks* **1994**, *2*, 239−245.
(29) Martin, J. E.; Adolf, D.; Wilcoxon, J. P. Viscoelasticity of near-critical gels. *Phys. Rev. Lett.* **1988**, *61*, 2620−2623.
(30) Corrigan, A. M.; Donald, A. M. Particle tracking microrheology of gel-forming amyloid fibril networks. *Eur. Phys. J. E* **2009**, *28*, 457−462.
(31) Adams, D. J.; Mullen, L. M.; Berta, M.; Chen, L.; Frith, W. J. Relationship between molecular structure, gelation behaviour and gel properties of Fmoc-dipeptides. *Soft Matter* **2010**, *6*, 1971−1980.
(32) Kocienski, P. *Protecting Groups*; Thieme Foundations of Organic Chemistry Series; G. Thieme: New York, 1994.
(33) Pocker, Y.; Green, E. Hydrolysis of D-glucono-δ-lactone. I. General acid-base catalysis, solvent deuterium isotope effects, and transition state characterization. *J. Am. Chem. Soc.* **1973**, *95*, 113−119.
(34) Savin, T.; Doyle, P. S. Static and dynamic errors in particle tracking microrheology. *Biophys. J.* **2005**, *88*, 623−638.
(35) Papagiannopoulos, A.; Waigh, T. A.; Hardingham, T. E. The viscoelasticity of self-assembled proteoglycan combs. *Faraday Discuss.* **2008**, *139*, 337−357.
(36) Hasnain, I. A.; Donald, A. M. Microrheological characterisation of anisotropic materials. *Phys. Rev. E* **2006**, *73*, 031901.
(37) Marr, D.; Hildreth, E. Theory of edge detection. *Proc. R. Soc. London, Ser. B* **1980**, *207*, 187−217.
(38) Dasgupta, B.; Tee, S.-Y.; Crocker, J. C.; Frisken, B. J.; Weitz, D. A. Microrheology of polyethylene oxide using diffusing wave spectroscopy and single scattering. *Phys. Rev. E* **2002**, *65*, 051505.
(39) Stauffer, D. Scaling theory of percolation clusters. *Phys. Rep.* **1979**, *54*, 1−74.
(40) Aufderhorst-Roberts, A.; Frith, W. J.; Donald, A. M. Micro-scale kinetics and heterogeneity of a pH triggered hydrogel. *Soft Matter* **2012**, *8*, 5940−5946.
(41) Rouse, P. E. J. A theory of the linear viscoelastic properties of dilute solutions of coiling polymers. *J. Chem. Phys.* **1953**, *21*, 1272−1280.
(42) Zimm, B. H. Dynamics of polymer molecules in dilute solution: viscoelasticity, flow birefringence and dielectric loss. *J. Chem. Phys.* **1956**, *24*, 269−278.
(43) Gittes, F.; MacKintosh, F. Dynamic shear modulus of a semiflexible polymer network. *Phys. Rev. E* **1998**, *58*, R1241.
(44) Ross-Murphy, S. B. Biopolymer gelation- exponents and critical exponents. *Polym. Bull.* **2007**, *58*, 119−126.
(45) Mason, T. G.; Gang, H.; Weitz, D. A. Diffusing-wave-spectroscopy measurements of viscoelasticity of complex fluids. *J. Opt. Soc. Am. A* **1997**, *14*, 139−149.
(46) MacKintosh, F.; Käs, J.; Janmey, P. Elasticity of semiflexible biopolymer networks. *Phys. Rev. Lett.* **1995**, *75*, 4425.
(47) Palmer, A.; Mason, T. G.; Xu, J.; Kuo, S. C.; Wirtz, D. Diffusing wave spectroscopy microrheology of actin filament networks. *Biophys. J.* **1999**, *76*, 1063−1071.
(48) Thornton, K.; Smith, A. M.; Merry, C. L.; Ulijn, R. V. Controlling stiffness in nanostructured hydrogels produced by enzymatic dephosphorylation. *Biochem. Soc. Trans.* **2009**, *37*, 660−664.
(49) Ozbas, B.; Rajagopal, K.; Schneider, J. P.; Pochan, D. J. Semiflexible chain networks formed via self-assembly of β-hairpin molecules. *Phys. Rev. Lett.* **2004**, *93*, 268106.
(50) Carrick, L.; Tassieri, M.; Waigh, T. A.; Aggeli, A.; Boden, N.; Bell, C.; Fisher, J.; Ingham, E.; Evans, R. M. L. The internal dynamic modes of charged self-assembled peptide fibrils. *Langmuir* **2005**, *21*, 3733−3737.
(51) Hamley, I. W.; Krysmann, M. J.; Newby, G. E.; Castelletto, V.; Noirez, L. Orientational ordering in the nematic phase of a polyethylene glycol−peptide conjugate in aqueous solution. *Phys. Rev. E* **2008**, *77*, 062901.
(52) Williams, R. J.; Smith, A. M.; Collins, R.; Hodson, N.; Das, A. K.; Ulijn, R. V. Enzyme-assisted self-assembly under thermodynamic control. *Nat. Nanotechnol.* **2009**, *4*, 19−24.

(53) Aufderhorst-Roberts, A. Microrheological Characterisation of Fmoc Derivative Hydrogels. Ph.D. Thesis, Wolfson College, University of Cambridge, 2012.